ARTICLE

Support for a synaptic chain model of neuronal sequence generation

Michael A. Long[1]†, Dezhe Z. Jin[2] & Michale S. Fee[1]

In songbirds, the remarkable temporal precision of song is generated by a sparse sequence of bursts in the premotor nucleus HVC. To distinguish between two possible classes of models of neural sequence generation, we carried out intracellular recordings of HVC neurons in singing zebra finches (*Taeniopygia guttata*). We found that the subthreshold membrane potential is characterized by a large, rapid depolarization 5–10 ms before burst onset, consistent with a synaptically connected chain of neurons in HVC. We found no evidence for the slow membrane potential modulation predicted by models in which burst timing is controlled by subthreshold dynamics. Furthermore, bursts ride on an underlying depolarization of ~10-ms duration, probably the result of a regenerative calcium spike within HVC neurons that could facilitate the propagation of activity through a chain network with high temporal precision. Our results provide insight into the fundamental mechanisms by which neural circuits can generate complex sequential behaviours.

Complex behaviours are made possible by the ability of the brain to step through well defined sequences of neural states[1]. Brain processes capable of generating intrinsic sequential activity are thought to underlie motor sequencing[2], navigation[3,4], movement planning[5], sensitivity to the timing of sensory stimuli[6] and cognitive tasks[7]. With few exceptions[8], however, the biophysical mechanisms by which neural circuits produce sequences are poorly understood.

Songbirds have emerged as an excellent model system for investigating the neural mechanisms of sequence generation. The adult zebra finch song motif consists of a stereotyped pattern of song syllables[9]. One premotor forebrain area in particular, nucleus HVC (used as a proper name), is known to have a central role in controlling the temporal structure of birdsong[10–12]. During singing, neurons in HVC projecting to downstream premotor nucleus RA (robust nucleus of the arcopallium) produce only a single highly stereotyped burst of spikes during each repetition of the song motif[13]. Different RA-projecting HVC neurons (HVC$_{(RA)}$) burst at different time points in the song, indicating that HVC neurons may burst sequentially through the song motif, in turn activating a complex and highly stereotyped pattern of bursts in the downstream nucleus RA[14,15].

Here we set out to distinguish experimentally among several distinct classes of possible sequence-generating circuits within HVC. First, it has been proposed that sequential states of neural activity may be generated by synaptically connected chains of neurons[6,16,17]. In this view, activity could propagate through the HVC network—like a chain of falling dominoes—forming the basic clock that underlies song timing (Fig. 1a)[10,18–20]. A second, fundamentally different, class of models can allow for sequence generation in the absence of overt feed-forward connections between HVC$_{(RA)}$ neurons. In these models, oscillatory or other subthreshold dynamics can modulate the excitability of neurons and thus control the timing of their activity[21,22], like those proposed to control the sequential activation of spikes during hippocampal theta sequences[23] and within replay events[3,24]. Subthreshold dynamics and rhythmicity on the timescale of song syllables (~100 ms) exist within HVC *in vitro*[25] and thus could have a central

role in controlling the timing of HVC bursts on that timescale in the singing bird.
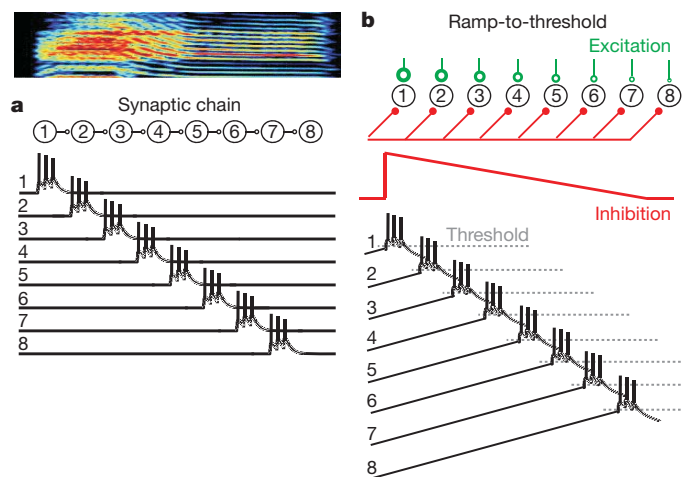
Figure 1 | Two broad classes of models for a sequence-generating circuit. a, Neurons might form a feed-forward synaptically connected chain within the HVC such that activity propagates from one group of neurons to the next. **b,** Alternatively, sequential activity might occur in the absence of directed connections between neurons, from temporal and spatial gradients of excitability. For example, the network could receive a global and gradual ramping-down of an inhibitory input over time (red synapses), producing a sequential activation. The order of activation would be determined by neuronal excitability. In the example model shown here, neurons receive different levels of constant excitatory input (green synapses). The neuron with the largest excitatory input (neuron 1) would be most depolarized and would be the first to reach spiking threshold. The neuron with the smallest constant excitatory input (neuron 8) would be the last to reach threshold. In the model depicted here, the timescale of the sequence produced corresponds to one song syllable (shown above).

[1]McGovern Institute for Brain Research, Department of Brain and Cognitive Sciences, Massachusetts Institute of Technology, 77 Massachusetts Avenue, Cambridge, Massachusetts 02139, USA. [2]Department of Physics, The Pennsylvania State University, University Park, Pennsylvania 16802, USA. †Present address: Departments of Otolaryngology and Physiology and Neuroscience, NYU School of Medicine, 522 First Avenue, New York, New York 10016, USA.

Intracellular recording during singing

To examine the role of subthreshold dynamics in the control of timing of HVC bursts during singing, we adopted an approach recently introduced for intracellular recordings in the freely moving rat[26]. We developed a miniature (1.6 g) microdrive that allows sharp microelectrode recordings to be performed in singing male zebra finches (Fig. 2a). Birds could move freely in a recording chamber, unrestrained except for a thin, flexible tether. In total, 28 neurons in 12 birds were recorded during singing of all three HVC neuron types, defined broadly by their axonal projections[27,28] (Fig. 2b).

The singing-related spiking patterns of intracellularly recorded neurons closely resembled the previously described patterns in extracellular recordings[13,29]. Putative interneurons ($n = 3$) were identified by a high spontaneous firing rate, and a continuous high firing rate throughout song (Fig. 2c, 117 ± 24.6 Hz singing, 66.3 ± 21.6 Hz baseline, error bars indicate $\pm$s.e.m. unless otherwise noted). Putative HVC neurons projecting to the basal ganglia homologue area X ($n = 12$) exhibited a low spontaneous spiking rate (<10 Hz) when the bird was not singing, and one or more high-frequency bursts during singing (Fig. 2d). These neurons showed a gradual hyperpolarization during the introductory notes (before the first motif in a bout of singing), and were hyperpolarized during song motifs (Fig. 2d, $n = 12$ of 12 cells; singing, -70.8 ± 3.4 mV; baseline, -67.7 ± 3.1 mV), similar to what has been observed during auditory song playback[30,31]. We did not consider these neurons further in the context of sequence generation because it has been shown that selective ablation of X-projecting HVC neurons in adult zebra finches does not impair song production[32].

HVC neurons that project to RA were identified by antidromic stimulation from RA (Fig. 2e, inset; see also Supplementary Fig. 1)[13]. HVC(RA) neurons showed a gradual depolarization before the onset of singing (Fig. 2e) and were persistently depolarized during singing ($n = 13$ of 13 cells; singing, -67.3 ± 3.5 mV; baseline, -75.7 ± 3.5 mV). About half of HVC(RA) neurons ($n = 7$ of 13) generated a single burst during each song motif (Fig. 3a–c, 3.8 ± 0.6 spikes per burst). The remaining HVC(RA) neurons ($n = 6$ of 13 cells) did not spike during song motifs (for example, Fig. 3d)[13].

## Chain model versus ramp-to-threshold model

Recurrent synaptic connections within a network of sequentially active neurons would be expected to produce patterned synaptic inputs; thus previous reports of patterned synaptic inputs have been used as evidence of synaptically connected chains both *in vitro* and *in vivo*[33]. Consistent with this view, we observed a highly stereotyped pattern of fast subthreshold fluctuations widely distributed throughout the song (Figs 2e and 3a–d, and Supplementary Fig. 2). For individual neurons, the song-aligned subthreshold fluctuations were highly correlated across song motifs (cross-correlation 0.80 ± 0.04, $P < 10^{-9}$, $n = 13$ neurons).

We now ask whether, as predicted by the ramp-to-threshold model, there was any slow ramping of membrane potential before the onset of bursts (Fig. 1b). We first consider the time window from the beginning of the song motif to the burst onset for each neuron. Across all 7 HVC(RA) neurons that burst during singing, the membrane potential did not change significantly in the period from the beginning of the
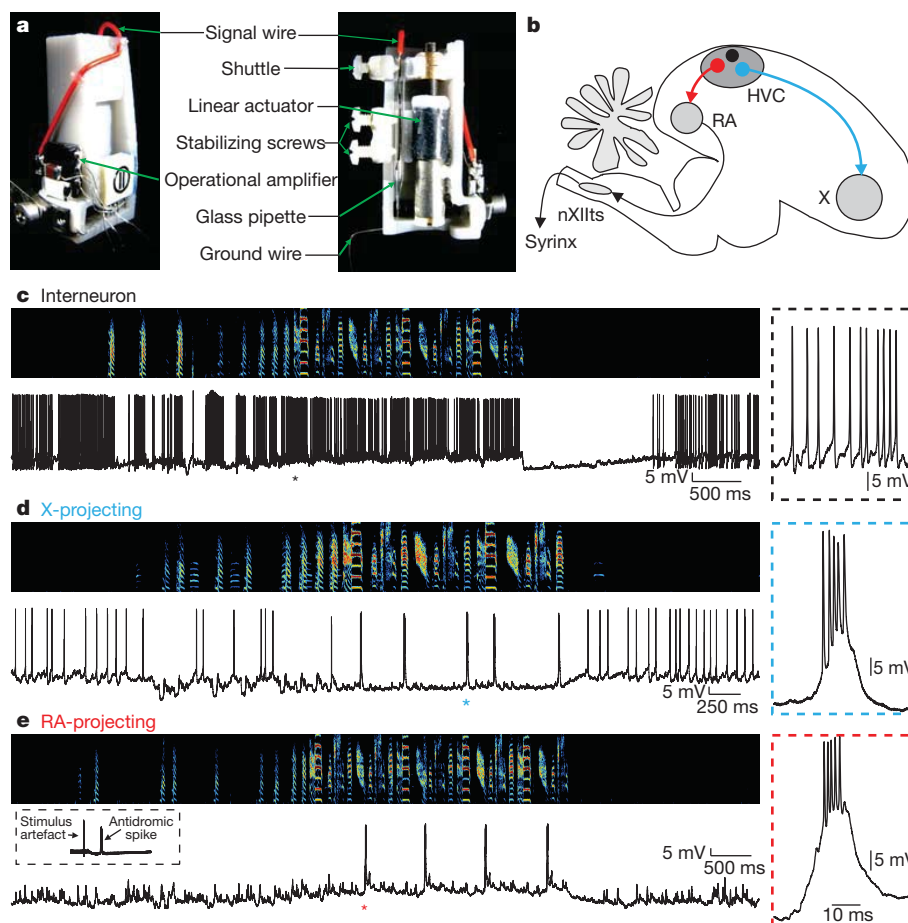
Figure 2 | A microdrive for sharp intracellular recording in the singing bird. a, The intracellular microdrive incorporates a motor that rotates a threaded rod and advances a shuttle that holds the electrode. **b**, A schematic of the zebra finch brain, highlighting three cell types in nucleus HVC defined by their projections: local circuit interneurons (in black), neurons that project to RA (in red), and neurons that project to basal-ganglia-homologue area X (in blue). **c–e**, Examples of intracellular records from a putative local circuit interneuron (**c**), a putative X-projecting neuron (**d**) and an antidromically identified RA-projecting neuron (**e**). Asterisk indicates the region magnified in the panels to the right.
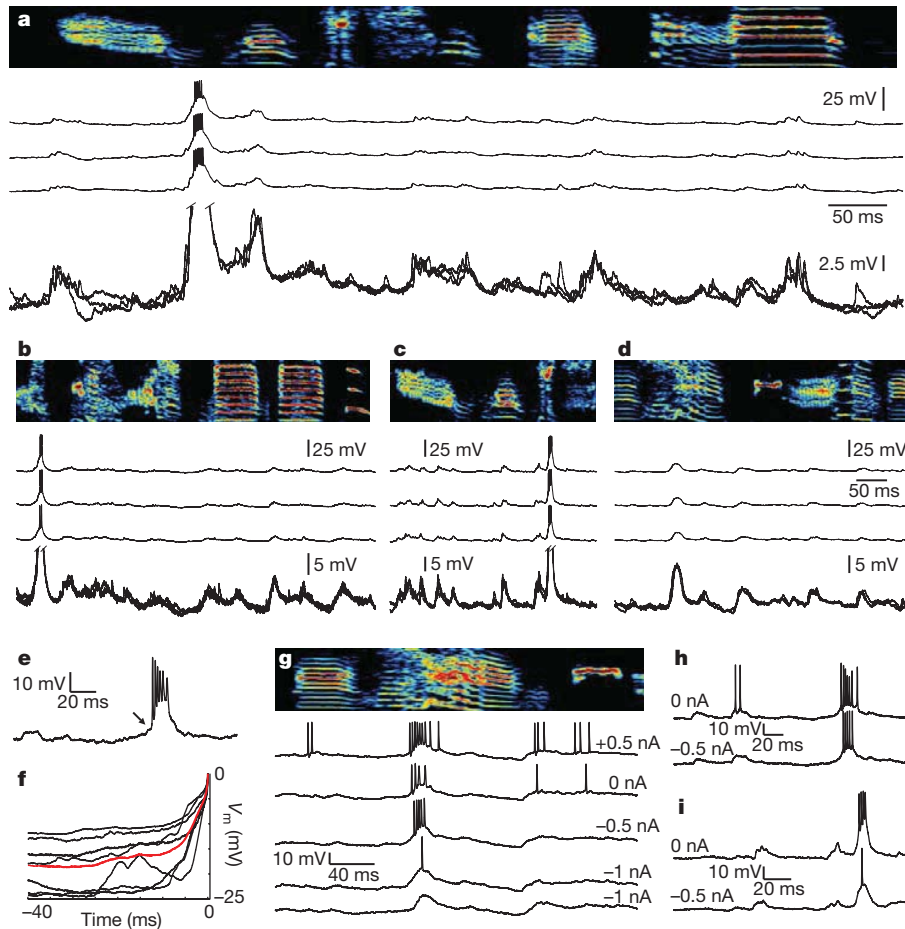
Figure 3 | Intracellular membrane potential of identified HVC$_{(RA)}$ neurons during singing. a–d, Examples of the membrane potential of four HVC$_{(RA)}$ neurons recorded during singing. For each cell, activity from three motif renditions is shown aligned to the song (top). Also shown is an overlay of the membrane potential traces (expanded vertical scale, bottom of each panel). **e**, Expanded view of a burst from another neuron during singing showing the flat membrane potential before burst onset (arrow). **f**, Average membrane

potential of seven HVC$_{(RA)}$ neurons before the first spike in the burst (time zero). The population average is shown in red. **g–i**, The membrane potential of three HVC$_{(RA)}$ neurons during singing with different holding currents. **g**, One neuron was held long enough to record with injected currents of +0.5 nA, 0 nA, −0.5 nA and −1.0 nA. **h, i**, Two other neurons recorded with 0 nA and −0.5 nA hyperpolarizing current. Note that injected current had little effect on burst timing, inconsistent with the predictions of the ramp-to-threshold model.

song motif to the moment 10 ms before the first spike in the burst (−0.47 ± 0.69 mV, $P = 0.53$, t-test, average window duration, 387 ± 92 ms). We next considered a ramp of excitation on the shorter timescale of a song syllable (~100 ms). Across all bursting neurons ($n = 7$), the membrane potential did not change during a window from 100 ms to 10 ms before the first spike in the burst (0.31 ± 1.04 mV, $P = 0.77$, t-test). Both of these results are inconsistent with a slow ramp of excitation before burst onset, on the timescale of either a song motif or a song syllable. In contrast, bursts of HVC$_{(RA)}$ neurons were preceded, within the 5 ms before the first spike in the burst, by a large depolarization of 10.5 ± 1.9 mV from baseline (Fig. 3e, f, the first spike of the burst initiated at a membrane potential of −52.6 ± 1.7 mV). This result is consistent with a model in which HVC$_{(RA)}$ neurons are activated by a large synchronous synaptic input from a group of previously active neurons.

The two models described in Fig. 1 give very different predictions for the effect of intracellular current injection on the timing of neural activity. In a model in which the timing of HVC$_{(RA)}$ bursts is controlled by slow membrane potential dynamics (Fig. 1b), an injected depolarizing current would cause the neuron to burst earlier during the slow depolarizing ramp, assuming that the burst-generating mechanism is sufficiently well coupled to the site of current injection (see Supplementary Discussion). In contrast, in the chain model, burst timing is controlled by a synaptic input from a preceding group of neurons (Fig. 1a). Thus, current injection would have a minimal

effect on burst timing, perhaps causing the first spike in the burst to appear a few milliseconds earlier during the onset of the synaptic depolarization.

We assessed the effect of intracellular current injection on the timing of bursts in HVC$_{(RA)}$ neurons during singing in three neurons. Two neurons were recorded with zero holding current and with 0.5 nA of hyperpolarizing current. One additional neuron was held long enough to record at four levels of holding current (0.5 nA, 0 nA, −0.5 nA and −1 nA). On average, the resulting membrane potential change was 20.3 mV nA^{-1} of injected current. In all cases, hyperpolarizing current was seen to reduce the number of spikes in the burst (Fig. 3g–i, average 5 spikes per burst at 0 nA compared to 3.3 spikes per burst at −0.5 nA), and could suppress spiking completely at the most hyperpolarizing currents (−1.0 nA). Depolarizing current injection increased the number of spikes per burst (Fig. 3g).

Remarkably, the timing of the burst was only weakly affected by injected currents. At a hyperpolarizing holding current of 0.5 nA, the burst onset was delayed by an average of only 2.6 ms ($n = 3$). However, the last spike of the burst was advanced by a similar amount such that the centre of the burst (midpoint between first and last spikes) was very weakly affected by injected current (1.2 ms nA^{-1}, Fig. 3g–i). In addition, under conditions at which the spiking was suppressed or nearly suppressed by hyperpolarizing current, a large underlying depolarization at the temporal position of the burst was clearly visible (Fig. 3g, i). These results are consistent with a mechanism in which a given

HVC$_{(RA)}$ neuron is driven by fast synaptic input from a preceding group of neurons.

Cellular mechanisms of burst generation

The broad powerful depolarizations that underlie the bursts of spikes in HVC$_{(RA)}$ neurons during singing (Fig. 3) are reminiscent of dendritic calcium spikes observed in many neurons[34,35]. Although it is difficult to establish definitively that the singing-related bursts of HVC$_{(RA)}$ neurons are mediated by calcium spikes, we have carried out *in vitro* and *in vivo* whole-cell recordings and pharmacological manipulations that support this view.

Although HVC$_{(RA)}$ neurons have not been observed to generate a burst response to somatic intracellular current injection (Fig. 4a, b)[27,28,36], dendritic calcium spikes in some neurons may not be observed during somatic current injection[37], but can be unmasked by the intracellular blockade of sodium and potassium channels[38]. We carried out whole-cell recordings in brain slices of antidromically identified HVC$_{(RA)}$ neurons with QX-314 in the recording pipette. Indeed, current injection resulted in a large depolarizing event in all neurons tested ($n = 23$ cells, Fig. 4c, average amplitude 26.4 ± 5.6 mV, width at half height 4.5 ± 1.0 ms). The depolarizing events had a clear all-or-none response with an initiation threshold at the soma of -36.2 ± 4.4 mV (Fig. 4d, $n = 14$ cells, compared to a threshold of -40.3 ± 4.3 mV for sodium spikes). In contrast, neurons in nucleus RA did not exhibit all-or-none spikes in the presence of QX-314 (ref. 39; Supplementary Fig. 3). The depolarizing events in HVC$_{(RA)}$ neurons were completely blocked by the broad spectrum calcium channel antagonist cadmium (100 µM, $n = 4$ cells), but were unaffected by nickel (100 µM, $n = 5$ cells), an antagonist of low-threshold voltage-gated calcium channels, indicating that the depolarizing events might be mediated by a high-threshold calcium channel.

We found that the L-type calcium channel agonist BAY K 8644 could enhance the calcium current sufficiently to evoke a burst response in HVC$_{(RA)}$ neurons even in the absence of QX-314 ($n = 8$ cells, Fig. 4e, f, average of 3.4 ± 0.2 spikes, within-burst spike rate 302 ± 14 Hz). These burst responses appeared to have an all-or-none characteristic with a well-defined threshold for injected current (0.50 ± 0.05 nA), and a spike rate within bursts that did not increase at higher currents ($P = 0.60$). These *in vitro* experiments indicate that HVC$_{(RA)}$ neurons are capable, under some conditions, of generating calcium-based regenerative spikes, possibly mediated by an L-type Ca conductance.

We wanted to examine more directly the role of these calcium conductances under conditions in which HVC$_{(RA)}$ neurons naturally generate burst sequences, rather than in brain slice. In a form of 'replay' of song-like patterns[40], HVC$_{(RA)}$ and RA neurons generate sparse sequential bursts during sleep similar to those produced during singing[13,41]. We have adapted a head-fixed sleeping bird preparation[13] and used whole-cell recordings and pharmacological manipulation of HVC$_{(RA)}$ neurons to study the mechanisms underlying these bursts in naturally sleeping zebra finches (Fig. 4g). Across the population of HVC$_{(RA)}$ neurons in our data set ($n = 36$ cells), nearly half the spikes recorded ($49.3 \pm 3.5\%$) formed high-frequency bursts (>100 Hz) during sleep (2.74 ± 0.11 sodium spikes, average within-burst rate of 265 ± 13 Hz). Just as during singing, sleep bursts were seen to ride on a prominent underlying depolarizing event (Fig. 4g, 25.2 ± 0.9 mV amplitude, 18.4 ± 1.5 ms width at 2/3 height).

Injections of the L-type calcium channel agonist BAY K 8644 (100 µM, 5–20 nl bolus) in the vicinity (<100 µm) of the whole-cell recording pipette increased the burst size (Fig. 4i, increased number of spikes and total burst duration, $P < 10^{-5}$ for both measures, Kolmogorov-Smirnov test). In addition, these injections significantly increased the incidence of bursting (Fig. 4k, mean interburst interval 2.0 ± 5.7 s with BAY K 8644, compared to 18.4 ± 34.5 s control, $P < 10^{-4}$, Kolmogorov-Smirnov test, $n = 6$ cells from 5 birds, mean ± s.d.). In contrast, injections of the L-type calcium channel antagonist nifedipine (100 µM) significantly decreased burst incidence (Fig. 4k,
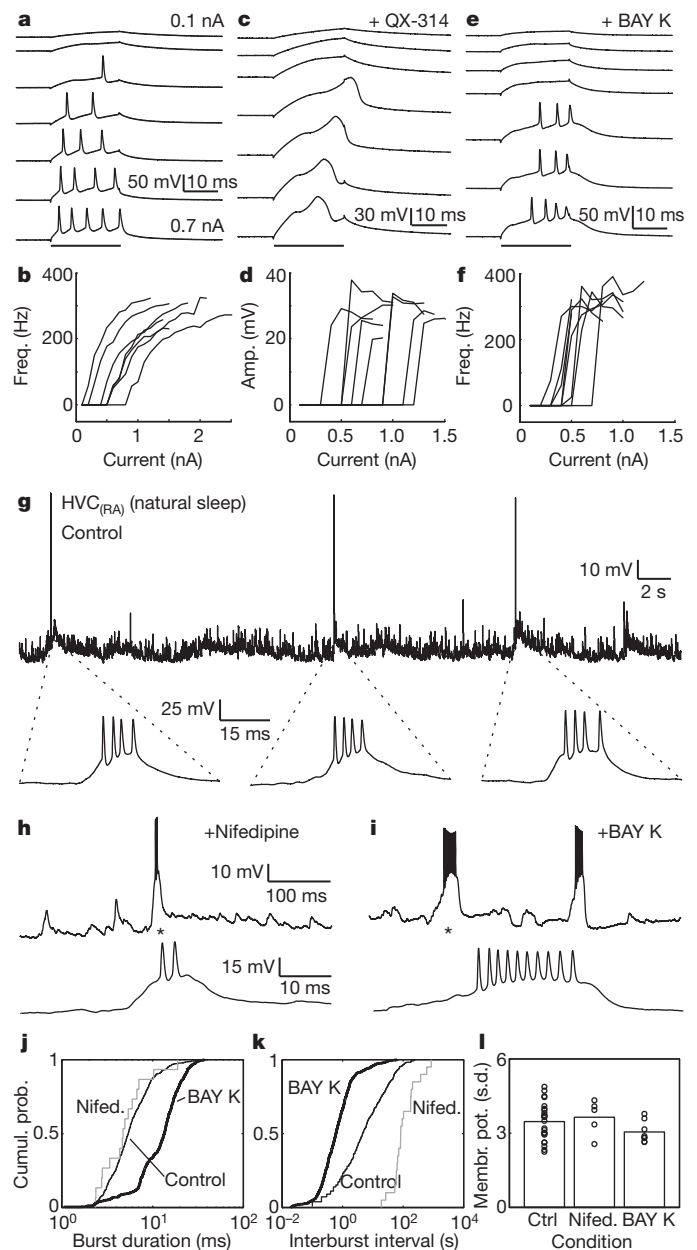
Figure 4 | Evidence that calcium channels contribute to burst events in HVC$_{(RA)}$ neurons. a, Response of an HVC$_{(RA)}$ neuron in brain slice to somatically injected current steps (black bar) of different size. **b**, Relationship between injected current and evoked firing rate in a population of 7 HVC$_{(RA)}$ neurons. Note that somatic current injection does not elicit an all-or-none burst. **c**, In the presence of intracellular sodium and potassium channel blocker QX-314 (5 mM), calcium spikes appear as an all-or-none depolarizing event. **d**, The amplitude of the depolarizing event (threshold to maximum point) as a function of injected current reveals an all-or-none response ($n = 8$ of 8 cells). **e, f**, HVC$_{(RA)}$ neurons treated with the L-type calcium channel agonist BAY K 8644 (5–10 µM) generate all-or-none spike bursts in response to somatic current injection. **g**, Segment of a whole-cell recording in a head-fixed bird during natural sleep showing three spontaneous bursts. **h, i**, Spontaneous bursting activity recorded during sleep after localized injection of L-type calcium channel antagonist nifedipine (**h**) or agonist BAY K 8644 (**i**). Asterisk indicates expanded view below. **j, k**, Cumulative distribution of burst durations and inter-burst intervals for control, nifedipine and BAY K 8644 conditions. **l**, Standard deviation of membrane potential fluctuations is not affected by nifedipine or Bay K 8644, indicating that synaptic transmission is not affected by these drugs.
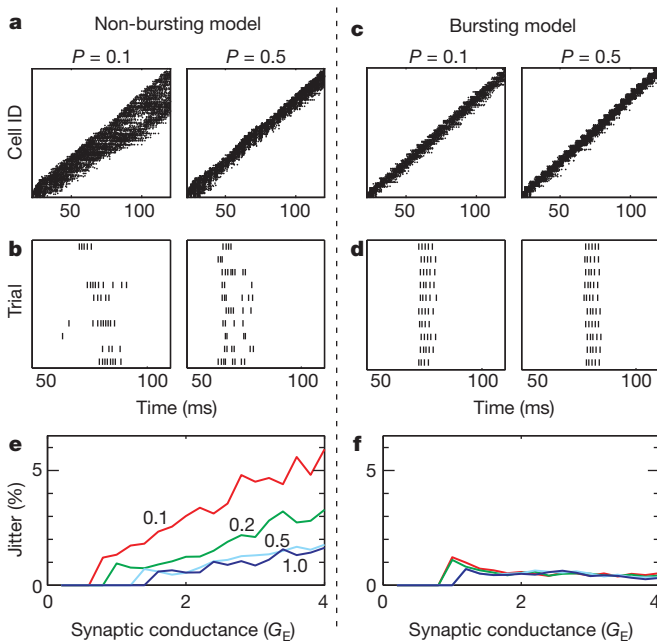
mean interburst interval 171.7 ± 209.6 s, greater than control, $P < 0.0001$, Kolmogorov-Smirnov test, $n = 6$ cells from 4 birds, mean ± s.d.). The effect of L-type calcium channel modulators could

not be explained by changes in the size of synaptic inputs: the magnitude of fluctuations in membrane potential was not altered by BAY K 8644 or nifedipine ($P > 0.05$, t-test, Fig. 4l). Taken together, these experiments demonstrate that L-type calcium channels have a role in generating or initiating bursting activity in $HVC_{(RA)}$ neurons. Such highly nonlinear all-or-none calcium spikes produce a highly stereotyped response to a wide range of synaptic inputs[42], and could have implications for the propagation of activity in a synaptically connected chain of neurons.

Burst propagation in a chain network

The stable propagation of bursts in an excitatory chain network is non-trivial; it requires precisely tuned synaptic strengths to avoid runaway excitation or decay[19]. It has previously been shown that an intrinsic neuronal burst mechanism can allow the stable propagation of activity in a chain network[19], but what about temporal precision and stereotypy? Here we use a simple biophysical model to examine the role that intrinsic bursting might have in achieving precise stereotyped temporal structure in the presence of noise. We also examine how such a mechanism might make the functioning of these networks robust over a wide range of network and synaptic properties.

We studied a network of 70 groups of 30 excitatory $HVC_{(RA)}$ neurons each, organized in a sequentially connected chain. Recurrent inhibition in HVC[25,43] was implemented by a population of 300 interneurons with sparse random connections to the excitatory chain (Supplementary Fig. 4a). We began with a non-bursting model of $HVC_{(RA)}$ neurons, described by a single spiking somatic compartment (Fig. 5, Supplementary Fig. 4b and Supplementary Methods).

We found that this network did not exhibit the unstable (explosive or decaying) behaviour characteristic of purely excitatory networks[19], but exhibited stable propagation of burst activity over a wide range of connection probabilities ($P = 0.1$–1.0) and excitatory synaptic strengths between $HVC_{(RA)}$ neurons in successive groups ($G_{EE,max}$ from 0.2 to 4.0 mS cm^{-2}). Nevertheless, the activity tended to be non-stationary, particularly at lower connection probabilities ($P = 0.1$, Fig. 5a), exhibiting both dispersion (broadening) and variations in propagation velocity at different points in the network (Supplementary Figs 5 and 6a, b). Furthermore, the network was sensitive to the presence of noise, producing activity that was not stereotyped across multiple trials of the simulation, including large jitter in the speed of propagation through the network (Fig. 5b, e; $1.95 \pm 1.38\%$ mean run-time jitter $\pm$ s.d.) and large variations in the burst response on different trials (quantified as spikes per burst and burst unreliability, Supplementary Fig. 6c–e). Finally, many characteristics of the propagation (number of spikes per burst, burst duration and burst jitter) were strongly dependent on the network connection probabilities and connection strengths (Fig. 5 and Supplementary Fig. 6). Thus, although the stable propagation of bursts is possible in a chain network of non-bursting neurons, the network does not produce the stereotyped sequences characteristic of real $HVC_{(RA)}$ neurons.

The situation was markedly different in a model with neurons that have an intrinsic burst mechanism. Bursting $HVC_{(RA)}$ neurons were modelled with a spiking somatic compartment plus a dendritic compartment containing conductances for generating calcium spikes (see Supplementary Figs 4c, d and 7–9). Propagation down the chain was stationary, with no broadening or variations in velocity (Fig. 5c and Supplementary Fig. 5). The propagation was also extremely stereotyped, exhibiting small trial-to-trial variations in propagation speed (Fig. 5d, $0.52 \pm 0.17\%$ mean run-time jitter $\pm$ s.d.). Burst response was much more reliable in the bursting model (see spikes per burst and burst unreliability, Supplementary Fig. 6), similar to what has been observed in singing-related firing patterns of $HVC_{(RA)}$ neurons[13,29]. Finally, in the bursting model, every characteristic of burst propagation that we examined was much more robust to variations in network connection probability and synaptic strength than was the single compartment model (Fig. 5e, f and Supplementary Fig. 6). Similar results were obtained with a simple integrate-and-burst model (Supplementary Fig. 10). Taken together, these results indicate that an intrinsic neuronal burst mechanism, regardless of its biophysical implementation, could serve a fundamental role in allowing synaptically connected chain networks to propagate in a highly stereotyped manner with low temporal jitter, even in the presence of noise, and over a wide range of network connectivities. Such robustness could also make sequence-generating networks easier to assemble during development[44,45].

We have carried out intracellular recording and manipulation of activity in the freely behaving animal in a neural circuit important for the temporal control of behaviour. We observed no ramping or rhythmicity that could contribute to the temporal patterning of $HVC_{(RA)}$ bursts. In contrast, our recordings reveal a single large postsynaptic potential that immediately precedes the onset of a song-locked burst of spikes. Together, our findings are consistent with the idea that the control of song temporal structure is produced by the propagation of calcium-mediated bursts through a synaptically connected chain of neurons. Temporally precise learned behaviours in other vertebrates could use similar mechanisms to organize neuronal activity into sequentially active states.

Figure 5 | A simple biophysical model to examine the implications of neuronal bursting on the robustness of HVC network propagation.
a–d, Two models of a synaptically connected chain network were compared: one with non-bursting neurons (**a**, **b**), the other with bursting neurons (**c**, **d**). **a**, Non-bursting model: spike raster plot for all neurons in the network showing activity as a function of time for two different levels of network connection probability ($P = 0.1$ and 0.5). **b**, Spike raster of a single neuron during different runs of the network. Note the non-stationarity of propagation and large variability across runs. **c**, Bursting model: spike raster plot for all neurons in the network. **d**, Spike raster of a single neuron during different runs of the network. Note the highly uniform propagation and stereotyped response across runs. **e**, **f**, Run-time jitter, plotted as a function of network connectivity and synaptic conductance, is consistently lower in the bursting model than in the non-bursting model. (See Supplementary Figures and Table for further quantification, and Supplementary Methods for model details.)

METHODS SUMMARY

Subjects. We used adult (>120 days post hatch) male zebra finches (*Taeniopygia guttata*). All animal procedures were reviewed and approved by the MIT committee on animal care.

Intracellular recording during singing. Intracellular recordings were achieved in the zebra finch using a custom microdrive constructed out of 3D printed plastic (AP Proto) outfitted with a lightweight linear actuator (Smoovy Series 0515,

Faulhaber). A preamplifier was mounted at the base of the device which routed signals to a commercially available intracellular amplifier (IR-183, Cygnus Technology). Sharp microelectrodes were pulled to a final impedance of 80–110 MΩ and were filled with 3 M potassium acetate. Once a stable intracellular recording was obtained, a female bird was presented to elicit directed singing.

Intracellular recording during sleep. During an initial surgical step, a stainless steel headplate was affixed to the skull. A small (~200 μm) craniotomy was made over HVC. Whole-cell recordings were made with glass electrodes (5–8 MΩ) using techniques described elsewhere[46]. Signals were measured using an Axoclamp 2B (Molecular Devices). In some experiments, an injection pipette (20–30 μm opening) was positioned less than 100 μm from the recording site for the injection (Nanoject II, Drummond Scientific) of a small volume (5–20 nl) of 100 μM (+/−)-BAY K 8644 (A.G. Scientific) or 100 μM nifedipine (Sigma).

Slice preparation. 400-μm slices were prepared on a vibrating microtome (Leica VT1000) and placed in ice-cold ACSF (sodium replaced with equimolar sucrose). Slices were then recorded in an interface-style chamber (VB5000, Leica) with standard ACSF (in mM): 126 NaCl, 3 KCl, 1.25 NaH$_2$PO$_4$, 2 MgSO$_4$-7H$_2$O, 26 NAHCO$_3$, 10 dextrose, 2 CaCl$_2$-2H$_2$0. QX-314 (5 mM, internal) was used in a subset of these experiments.

1. Lashley, K. in *Cerebral Mechanisms in Behavior* (ed. Jeffress, L.) (Wiley, 1951).
2. Shima, K., Isoda, M., Mushiake, H. & Tanji, J. Categorization of behavioural sequences in the prefrontal cortex. *Nature* **445,** 315–318 (2007).
3. Mehta, M. R., Lee, A. K. & Wilson, M. A. Role of experience and oscillations in transforming a rate code into a temporal code. *Nature* **417,** 741–746 (2002).
4. Harvey, C. D., Collman, F., Dombeck, D. A. & Tank, D. W. Intracellular dynamics of hippocampal place cells during virtual navigation. *Nature* **461,** 941–946 (2009).
5. Pastalkova, E., Itskov, V., Amarasingham, A. & Buzsaki, G. Internally generated cell assembly sequences in the rat hippocampus. *Science* **321,** 1322–1327 (2008).
6. Mauk, M. D. & Buonomano, D. V. The neural basis of temporal processing. *Annu. Rev. Neurosci.* **27,** 307–340 (2004).
7. Georgopoulos, A. P., Lurito, J. T., Petrides, M., Schwartz, A. B. & Massey, J. T. Mental rotation of the neuronal population vector. *Science* **243,** 234–236 (1989).
8. Stent, G. S. *et al.* Neuronal generation of the leech swimming movement. *Science* **200,** 1348–1357 (1978).
9. Konishi, M. Birdsong: from behavior to neuron. *Annu. Rev. Neurosci.* **8,** 125–170 (1985).
10. Long, M. A. & Fee, M. S. Using temperature to analyse temporal dynamics in the songbird motor pathway. *Nature* **456,** 189–194 (2008).
11. Yu, A. C. & Margoliash, D. Temporal hierarchical control of singing in birds. *Science* **273,** 1871–1875 (1996).
12. Vu, E. T., Mazurek, M. E. & Kuo, Y. C. Identification of a forebrain motor programming network for the learned song of zebra finches. *J. Neurosci.* **14,** 6924–6934 (1994).
13. Hahnloser, R. H., Kozhevnikov, A. A. & Fee, M. S. An ultra-sparse code underlies the generation of neural sequences in a songbird. *Nature* **419,** 65–70 (2002).
14. Leonardo, A. & Fee, M. S. Ensemble coding of vocal control in birdsong. *J. Neurosci.* **25,** 652–661 (2005).
15. Fee, M. S., Kozhevnikov, A. A. & Hahnloser, R. H. Neural mechanisms of vocal sequence generation in the songbird. *Ann. NY Acad. Sci.* **1016,** 153–170 (2004).
16. Amari, S. Learning patterns and pattern sequences by self-organizing nets of threshold elements. *IEEE Trans. Comp.* **c-21,** 1197–1206 (1972).
17. Abeles, M. *Corticonics: Neural Circuits of the Cerebral Cortex* (Cambridge Univ. Press, 1991).
18. Li, M. & Greenside, H. Stable propagation of a burst through a one-dimensional homogeneous excitatory chain model of songbird nucleus HVC. *Phys. Rev. E* **74,** 011918 (2006).
19. Jin, D. Z., Ramazanoglu, F. M. & Seung, H. S. Intrinsic bursting enhances the robustness of a neural network model of sequence generation by avian brain area HVC. *J. Comput. Neurosci.* **23,** 283–299 (2007).
20. Glaze, C. M. & Troyer, T. W. Behavioral measurements of a temporally precise motor code for birdsong. *J. Neurosci.* **27,** 7631–7639 (2007).
21. Mann, E. O. & Paulsen, O. Role of GABAergic inhibition in hippocampal network oscillations. *Trends Neurosci.* **30,** 343–349 (2007).
22. O'Keefe, J. & Recce, M. L. Phase relationship between hippocampal place units and the EEG theta rhythm. *Hippocampus* **3,** 317–330 (1993).
23. Foster, D. J. & Wilson, M. A. Hippocampal theta sequences. *Hippocampus* **17,** 1093–1099 (2007).
24. Buzsaki, G. Two-stage model of memory trace formation: a role for "noisy" brain states. *Neuroscience* **31,** 551–570 (1989).
25. Solis, M. M. & Perkel, D. J. Rhythmic activity in a forebrain vocal control nucleus *in vitro. J. Neurosci.* **25,** 2811–2822 (2005).
26. Lee, A. K., Manns, I. D., Sakmann, B. & Brecht, M. Whole-cell recordings in freely moving rats. *Neuron* **51,** 399–407 (2006).
27. Dutar, P., Vu, H. M. & Perkel, D. J. Multiple cell types distinguished by physiological, pharmacological, and anatomic properties in nucleus HVc of the adult zebra finch. *J. Neurophysiol.* **80,** 1828–1838 (1998).
28. Mooney, R. Different subthreshold mechanisms underlie song selectivity in identified HVc neurons of the zebra finch. *J. Neurosci.* **20,** 5420–5436 (2000).
29. Kozhevnikov, A. A. & Fee, M. S. Singing-related activity of identified HVC neurons in the zebra finch. *J. Neurophysiol.* **97,** 4271–4283 (2007).
30. Lewicki, M. S. Intracellular characterization of song-specific neurons in the zebra finch auditory forebrain. *J. Neurosci.* **16,** 5855–5863 (1996).
31. Rosen, M. J. & Mooney, R. Inhibitory and excitatory mechanisms underlying auditory responses to learned vocalizations in the songbird nucleus HVC. *Neuron* **39,** 177–194 (2003).
32. Scharff, C., Kirn, J. R., Grossman, M., Macklis, J. D. & Nottebohm, F. Targeted neuronal death affects neuronal replacement and vocal behavior in adult songbirds. *Neuron* **25,** 481–492 (2000).
33. Ikegaya, Y. *et al.* Synfire chains and cortical songs: temporal modules of cortical activity. *Science* **304,** 559–564 (2004).
34. London, M. & Hausser, M. Dendritic computation. *Annu. Rev. Neurosci.* **28,** 503–532 (2005).
35. Murayama, M. *et al.* Dendritic encoding of sensory stimuli controlled by deep cortical interneurons. *Nature* **457,** 1137–1141 (2009).
36. Kubota, M. & Taniguchi, I. Electrophysiological characteristics of classes of neuron in the HVc of the zebra finch. *J. Neurophysiol.* **80,** 914–923 (1998).
37. Larkum, M. E. & Zhu, J. J. Signaling of layer 1 and whisker-evoked Ca^{2+} and Na$^+$ action potentials in distal and terminal dendrites of rat neocortical pyramidal neurons *in vivo. J. Neurosci.* **22,** 6991–7005 (2002).
38. Connors, B. W. & Prince, D. A. Effects of local anesthetic QX-314 on the membrane properties of hippocampal pyramidal neurons. *J. Pharmacol. Exp. Ther.* **220,** 476–481 (1982).
39. Mooney, R. Synaptic basis for developmental plasticity in a birdsong nucleus. *J. Neurosci.* **12,** 2464–2477 (1992).
40. Dave, A. S. & Margoliash, D. Song replay during sleep and computational rules for sensorimotor vocal learning. *Science* **290,** 812–816 (2000).
41. Hahnloser, R. H., Kozhevnikov, A. A. & Fee, M. S. Sleep-related neural activity in a premotor and a basal-ganglia pathway of the songbird. *J. Neurophysiol.* **96,** 794–812 (2006).
42. Wei, D. S. *et al.* Compartmentalized and binary behavior of terminal dendrites in hippocampal pyramidal neurons. *Science* **293,** 2272–2275 (2001).
43. Mooney, R. & Prather, J. F. The HVC microcircuit: the synaptic basis for interactions between song motor and vocal plasticity pathways. *J. Neurosci.* **25,** 1952–1964 (2005).
44. Jun, J. K. & Jin, D. Z. Development of neural circuitry for precise temporal sequences through spontaneous activity, axon remodeling, and synaptic plasticity. *PLoS ONE* **2,** e723 (2007).
45. Fiete, I. R., Senn, W., Wang, C. Z. & Hahnloser, R. H. Spike-time-dependent plasticity and heterosynaptic competition organize networks to produce long scale-free sequences of neural activity. *Neuron* **65,** 563–576 (2010).
46. Margrie, T. W., Brecht, M. & Sakmann, B. *In vivo,* low-resistance, whole-cell recordings from neurons in the anaesthetized and awake mammalian brain. *Pflugers Arch.* **444,** 491–498 (2002).